Journal of Physics: Conference Series **3224** (2026) 032119 doi:10.1088/1742-6596/3224/3/032119

Assessment of wind turbine wake definitions for quantifying unsteady wake characteristics

Ali Ata Adam, Amanda S.M. Smyth, Christopher R. Vogel

Department of Engineering Science, University of Oxford, Oxford OX1 3PJ, UK

E-mail: ata.adam@eng.ox.ac.uk

Abstract. Mitigation of wake effects in wind farms often relies on predictive wake models, which are typically developed using parameters calibrated from transient wind turbine wake data. Therefore, accurate identification of instantaneous turbine wakes is essential for improving wind farm yield. Despite the wide range of proposed wake definitions, no consensus has been reached on a definition that is appropriate for characterising instantaneous wakes. This study presents a quantitative assessment of several commonly used wake definitions using a computational dataset of wind turbine wakes. The definitions are evaluated based on their ability to consistently identify the wake region and centre and to generate wake shapes that are physically consistent with turbine thrust. The results demonstrate that only a limited subset of the examined definitions is suitable for identifying unsteady wind turbine wakes, and that the choice of wake definition can significantly bias estimates of wake width expansion rate and wake meandering amplitude.

1. Introduction

Mitigating wake effects is crucial for wind farm operation because wind turbines operating in the wake of upstream turbines experience lower wind speeds, leading to reduced energy yield. Wind turbine wakes exhibit intrinsic instabilities, for example, from the shear layer, tip vortices, and hub vortices, that can trigger wake meandering [1, 2, 3] and amplify meandering driven by large-scale turbulent structures [4]. Furthermore, these instabilities govern the wake recovery rate by affecting momentum entrainment into the wake [5]. As a result, understanding and controlling wake instabilities and wake recovery mechanisms may lead to improved wind farm efficiency.

Accurate wake identification can help the development of control strategies and farm layout optimisation to reduce wake effects [6]. The evolution of wake parameters, such as the wake centre and width, has been widely investigated as they are often important variables in engineering wake models [7, 8]. Also, wake meandering is often quantified by the standard deviation of the lateral shift of the wake centre relative to the hub centreline [9].

Despite various proposed methods, a robust definition of a wake is challenging. The instantaneous far wake, of interest for unsteady analysis, typically exhibits an irregular shape and may not conform to a self-similar velocity profile [10, 11]. While some definitions are reported to perform well for unsteady wakes [10, 11, 12, 13, 14], systematic quantitative comparisons remain limited [13, 14], resulting from the absence of ground truth against which wake definitions can be validated. Most studies rely on qualitative assessments or relative agreement between methods rather than objective reference data [11, 12, 14]. Additional variability arises from definition

metrics, whose influence on wake parameters has not been quantitatively assessed. For instance, streamwise-velocity–based definitions commonly identify the wake using an iso-contour of the normalised velocity, yet the chosen threshold varies widely [5, 11, 14, 15].

This work provides a systematic assessment of commonly used wake definitions using a physically motivated and quantitatively defined evaluation framework applied to high-resolution Large Eddy Simulation (LES) datasets. The goal is to evaluate existing wake definitions and provide recommendations on their suitability for instantaneous wake characterisation. The main research questions addressed are: (i) to what extent widely used wake definitions are suitable for characterising instantaneous and unsteady wind turbine wakes, and (ii) whether definition variants affect the suitability of these definitions. Moreover, the assessment leads to discussions on the research question of (iii) how the choice of wake definition influences the quantification of unsteady wake characteristics.

2. Numerical simulations

This study uses a flow dataset generated by LES of the filtered, unsteady, incompressible 3D Navier-Stokes equations with the standard Smagorinsky turbulence closure, using the pressure-based solver `pimpleFoam` in the open-source software OpenFOAM. The transient terms in the governing equations are discretised using a second-order implicit backward time scheme. A cell-based linear Gauss scheme is used for gradient evaluation, and a second-order linear Gauss scheme is employed for the divergence terms. A constant time step of $\Delta t = 0.1$s is used, which ensures that the maximum Courant number remains well below unity.

The simulations are conducted in a computational domain of $24D \times 9D \times 9D$ (L×D×W), where the turbine rotor with a diameter of D is located at the centre of the yz-plane $4D$ downstream of the inlet. The most refined mesh region, where the cell size corresponds to 50 cells across the turbine diameter, extends from $1D$ upstream of the turbine to $15D$ downstream, ensuring that more than 80% of the turbulent kinetic energy is resolved in the far wake. A steady and uniform inflow is enforced at the inlet using a Dirichlet boundary condition. For the remaining boundary surfaces, symmetry boundary conditions are implemented.

The turbine rotor is modelled as an actuator disc (AD). A uniform thrust coefficient of $C_T = 0.8889$ is enforced on the disc. As shown in Fig. 1, this configuration leads to a near wake characterised by a coherent shear layer for $x/D < 5$, a transitional wake region for $5 < x/D < 10$ and a turbulent far wake for $x/D > 10$. Therefore, the robustness of the wake definitions can be assessed under different stages of a wind turbine wake. The relatively long transitional region is partly attributable to the AD, which does not shed blade-induced vortices, and to uniform inflow conditions that lack turbulence. Consequently, shear-layer instabilities grow and break down more gradually before a fully turbulent wake is established. Although an AD is not an entirely realistic representation of a wind turbine rotor due to the lack of discrete blades, it is known that the AD generates similar far wake characteristics to those of more realistic actuator models in practical mesh resolutions [16].

2.1. Actuator disc model

The in-house AD model represents the turbine rotor as a two-dimensional polar grid of collocation points. At each collocation point, the thrust force is projected onto the domain using a spherical Gaussian kernel. The smearing parameter, ε, is set to $\varepsilon = 2.5\Delta x$ where Δx is the isotropic cell size at the disc plane.

The numerical setup and the AD model are validated against the second porous-disc Round-Robin tests [17]. In this experimental campaign, the wake of a regular porous disc was measured

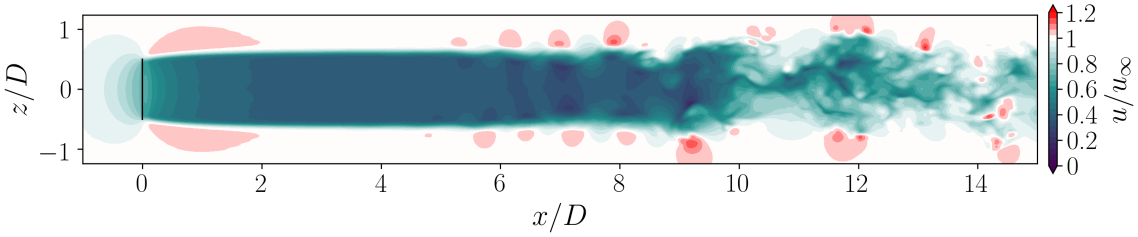

Figure 1. Instantaneous normalised streamwise velocity field on the $y = 0$ plane from the numerical dataset used in the wake definition assessment. The black vertical line at $x = 0$ represents the actuator disc.

in ten different wind tunnels at a diameter-based Reynolds number of $Re_D = 2 \times 10^5$. The low-turbulent inflow case is selected as the reference experiment, for which the freestream turbulence intensity ranges from 0.07% to 1.05% across the facilities [17].

The turbulent flow on the inlet boundary is generated using the Divergence Free Synthetic Eddy Method (DF-SEM) [18], which is calibrated to obtain an average turbulence intensity of 0.5% at the disc location. The thrust coefficient is set to $C_T = 0.77$, based on the force measurements reported in [19]. The time-averaged velocity profiles at hub height for $x/D = 4$ and $x/D = 8$ downstream locations are presented in Fig. 2, along with the range of the experimental measurements reported in [17]. Although the maximum velocity deficit at $x/D = 4$ is slightly underpredicted, the computational profiles largely overlap with the experimental range at both streamwise locations. In addition, the simulation accurately captures the transition from a near top-hat profile at $x/D = 4$ to a bell-shaped profile at $x/D = 8$.

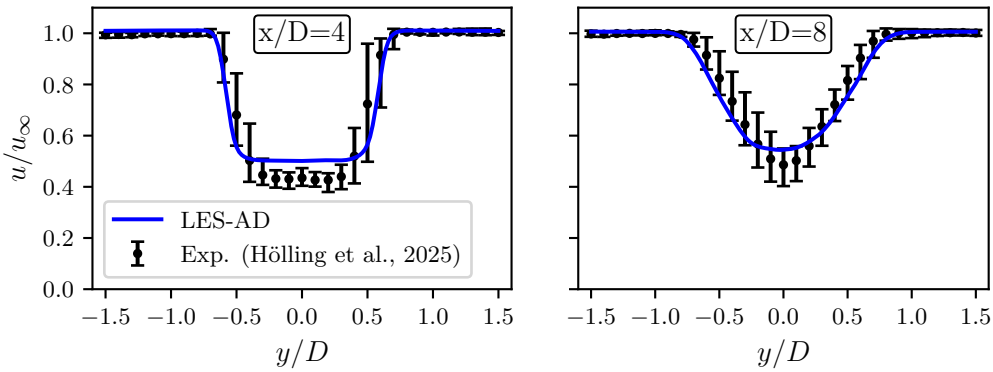

Figure 2. Time-averaged normalised streamwise velocity profile at hub height and (left) $x/D = 4$ and (right) $x/D = 8$ downstream of the disc for the AD model validation case. The average of experimental data from different institutions reported in [17] is indicated by circle markers, with error bars showing the range of the dataset for each available lateral location.

3. Wake definitions

A summary of the examined wake definitions, with their corresponding abbreviations used throughout the paper, is given in Table 1.

The VelT approach defines the wake boundary using streamwise velocity (u) contours of a user-specified factor of the freestream velocity at a wake cross-section. Similarly, a factor of the

Table 1. Summary of wake definitions considered in this paper, indicating the definition metrics and the wake parameters directly determined with each method.

Definition	Metrics	Wake border	Wake centre (c_y, c_z)	Effective wake width (W_{eff})
Velocity threshold (VelT)	u/u_∞	✓	✓	✓
Velocity deficit threshold (VelDefT)	$\Delta u/\Delta u_{\max}$	✓	✓	✓
Turbulence threshold (TT)	$k/k_{\max}$	✓	✓	✓
Gaussian fit (Gauss)	f_G & $W_{1/2}/\sigma$	✓	✓	✓
Centre of mass (CoM)	n		✓	
Centre of minimum available power (MinP)	-		✓	

maximum velocity deficit ($\Delta u_{\max}$) can be used to determine the wake shape from velocity-deficit (Δu) contours in the VelDefT approach.

Wakes are characterised by increased turbulence compared to the freestream. The TT approach defines the wake shape using an iso-contour of the turbulent kinetic energy (k), with the threshold specified as a fraction of the local maximum turbulent kinetic energy.

For the above-mentioned approaches, which directly define the wake shape, the wake centre is defined as the centroid of the wake shape, and the effective wake width is computed as the diameter of an equivalent circle that encloses the same area as the wake shape.

The Gauss method is based on fitting a Gaussian function to the velocity deficit distribution to estimate the wake centre and effective wake width [13]. In this approach, an elliptical shape is assumed, centred at the peak of the Gaussian distribution and extending to a factor of the Gaussian variance. As a result, this approach provides both the wake centre and the effective wake width. Metrics of this approach include the Gaussian function f_G used in the regression and the wake half-width, $W_{1/2}$, based on a factor of the Gaussian function variance σ. The f_G could be a univariate one-dimensional (1D), univariate two-dimensional (2D) or bivariate two-dimensional (Biv.) Gaussian function.

The CoM method defines the wake centre as the weighted centre of the velocity deficit.

$$c_y(x) = \frac{\iint y(u-u_\infty)^n \mathrm{dS}}{\iint (u-u_\infty)^n \mathrm{dS}}, \quad c_z(x) = \frac{\iint z(u-u_\infty)^n \mathrm{dS}}{\iint (u-u_\infty)^n \mathrm{dS}}, \tag{1}$$

where n can be $n = 1$ [20], $n = 2$ [21], or $n = 3$ [22], corresponding to the centre of velocity deficit, momentum deficit, and power deficit, respectively.

MinP relies on available power at the cross-section of the wake flow. In this approach, the total available power within circles of diameter D centred at different locations on a downstream plane is considered. The centre of the circle with the lowest available power is taken as the wake centre for the given streamwise location [12].

4. Wake assessment methodology

In this study, the aim is to evaluate the ability of the wake definitions to identify the wake region and its centre reliably, and to provide wake shapes that are physically consistent with turbine operating conditions, assessed using a set of unified parameters. This includes a parameter related to the wake centre, χ_c, and to the wake shape, χ_w. These parameters represent the proportion of wakes at a given downstream location satisfying all corresponding criteria listed in Table 2 and therefore range from 0 to 1, with unity indicating that the wake always satisfies all the given criteria at that axial location. In this study, they are evaluated using 2,600 snapshots of the wind turbine wake.

The wake centre index, χ_c, quantifies the portion of wakes in which their lateral wake centre components lie within the turbine radius, consistent with experimentally reported bounds on wake centre displacement [23], and shift a physically feasible distance between consecutive snapshots ($\mathrm{d}c^{\Delta t}$). The latter must be less than one-tenth of turbine diameter for the timestep of the examined dataset to remain consistent with reported wake meandering amplitudes and wavelengths [24].

The wake shape index, χ_w, gives the proportion of the wake shapes satisfying a set of four criteria. These include the coverage of the characteristic wake extrema, namely the minimum streamwise velocity and maximum turbulent kinetic energy points, and an effective wake width not exceeding three times the turbine diameter to exclude unrealistically broad wake regions while allowing far-wake expansion observed in measurements [25] and previously adopted plausibility limits [26]. The index also checks the temporal smoothness of wake motion, defined as the intersection-over-union (IoU) between the wake shapes at consecutive time steps at the same axial location. The threshold for this criterion permits physically plausible wake deformation and displacement, based on the adopted $\mathrm{d}c^{\Delta t}$ threshold for χ_c, while preventing discontinuous wake identification. The last criterion for χ_w is consistency with the streamwise momentum balance. This is quantified by the momentum balance factor, F_w/T, which assesses the physical consistency of the wake shape by evaluating whether it accounts for the rotor thrust when the streamwise momentum balance is applied over its volume within a prescribed tolerance of η_T reflecting modelling uncertainty. The following section explains how the momentum balance analysis is conducted, how F_w/T is evaluated, and how η_T is determined.

4.1. Momentum balance analysis

A momentum balance analysis is used to relate the flow field to the turbine thrust. Figure 3 shows the control volume used in this analysis, where the outlet coincides with the streamwise location of the analysed wake cross-section and the sides follow the wake boundary downstream of the turbine. This control volume yields a more complex momentum balance equation, including side-surface integral terms for the pressure force and momentum flux, than those used in the literature [27]. This definition ensures that the control volume completely covers the turbine even under a strongly unsteady wake. As a result, the momentum balance is satisfied against the turbine thrust when used along with an appropriate wake definition.

A complete momentum balance equation includes surface integrals over the side surfaces; however, accurate estimation of these integrals requires prohibitively high spatial resolution. To enable a practical formulation, a simplified momentum balance [27] is used,

$$F_w(x) = \iint_{\Gamma_w(x)} \left[u(u_\infty - u) - \frac{1}{\rho} p \right] \mathrm{d}\Gamma \approx \frac{1}{\rho} T \mathrm{H}(x), \tag{2}$$

Table 2. List of metrics and corresponding criteria used to construct the wake centre index (χ_c) and wake shape index (χ_w).

Index	Metric	Criteria
χ_c	Lateral wake centre position	$\lvert c_y\rvert/D \leq 0.5$ & $\lvert c_z\rvert/D \leq 0.5$
	Temporal wake centre shift	$\lvert \mathrm{d}c^{\Delta t} \rvert \leq 0.1D$
χ_w	Inclusion of wake extrema points	$u_{\min} \in \Gamma_w$ & $k_{\max} \in \Gamma_w$
	Effective wake width	$W_{\mathrm{eff}}/D \leq 3$
	Temporal wake shape intersection	$\mathrm{IoU} \geq 0.5$
	Momentum balance factor	$1 - \eta_T \leq F_w/T \leq 1 + \eta_T$

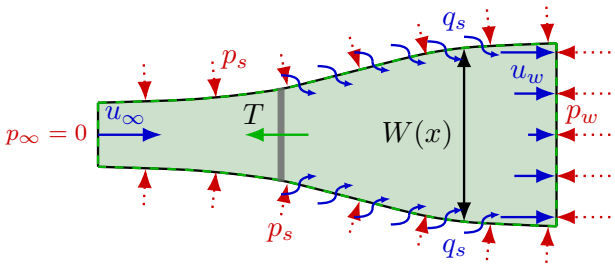

Figure 3. Control volume used in momentum balance analysis. The grey rectangle represents the wind turbine. The blue arrows represent the velocity, the red arrows show the pressure on the control surfaces, and the curved blue arrows indicate mass flux q_s through the side surfaces.

where Γ_w denotes the wake surface and $\mathrm{H}(x)$ is the Heaviside function. Applying Reynolds decomposition and time averaging leads to the steady formulation

$$\overline{F}_w(x) = \iint_{\Gamma_w(x)} \left[\overline{u}(u_\infty - \overline{u}) - \overline{u'u'} - \frac{1}{\rho}\overline{p}\right] \mathrm{d}\Gamma \approx \frac{1}{\rho}\overline{T}\mathrm{H}(x), \tag{3}$$

where for any variable $\phi = \overline{\phi} + \phi'$ with $\overline{\phi}$ and ϕ' are the time-averaged and fluctuating components, respectively.

For the considered control volume, the simplified momentum balance is obtained by assuming uniform and undisturbed flow at the inlet, and by substituting the following assumption,

$$\iint_{\Gamma_s} \left[u_\infty q - uq + \frac{1}{\rho} p n_x\right] \mathrm{d}\Gamma \approx 0, \tag{4}$$

where Γ_s stands for the side surface and the flow rate through the side boundaries is denoted by q which can be decomposed as $q = q_x + q_{yz}$ where $q_x = u n_{s,x}$ and $q_{yz} = v n_{s,y} + w n_{s,z}$. However, this assumption does not necessarily hold for turbulent wakes because the axial velocity and pressure along the wake boundaries may differ from their freestream and ambient values. Consequently, Eq. (2) or Eq. (3) may not hold for turbulent wakes either.

The residual arising from the simplified momentum balance formulation is determined using the time-averaged wake data. The residual is obtained by applying Reynolds decomposition and time averaging the left-hand side of Eq. (4) and evaluated over a control volume defined using the wake shape from an analytical AD model [28]. As this wake shape represents a plausible but non-unique definition of the wake boundary, the sensitivity of the residuals to the wake extent is assessed by scaling the wake width by a factor ranging from 0.8 to 1.2.

Figure 4 shows the streamwise evolution of the cumulative residual terms, with shaded regions indicating variability due to wake-width scaling. The residual remains bounded within approximately $\pm 0.2T$ over the streamwise range considered. Contributions from the streamwise turbulent momentum flux $\overline{u'q'_x}$ and side-surface pressure are negligible, while the dominant contributions arise from the $u = u_\infty$ assumption on Γ_s and the lateral turbulent momentum flux $\overline{u'q'_{yz}}$. The latter increases in magnitude monotonically downstream of $x/D \approx 10$, which coincides with the breakdown of the coherent shear layer, as shown in Fig. 1. Coherent wake structures inhibit energy entrainment into the wake [29], which explains why this term remains small for $x/D < 10$. Thus, wake definitions based solely on matching momentum deficit to rotor thrust [10, 13] may be insufficient, as they neglect momentum fluxes through the side boundaries.

The simplified momentum balance in Eq. (3) cannot therefore be expected to hold strictly in the far wake. To account for the residuals, a tolerance η_T is introduced in the assessment

with the momentum balance factor F_w/T, which is required to remain within $\pm\eta_T$ around the thrust value. Based on the observed residuals, the tolerance is set to $\eta_T = 0.2$.

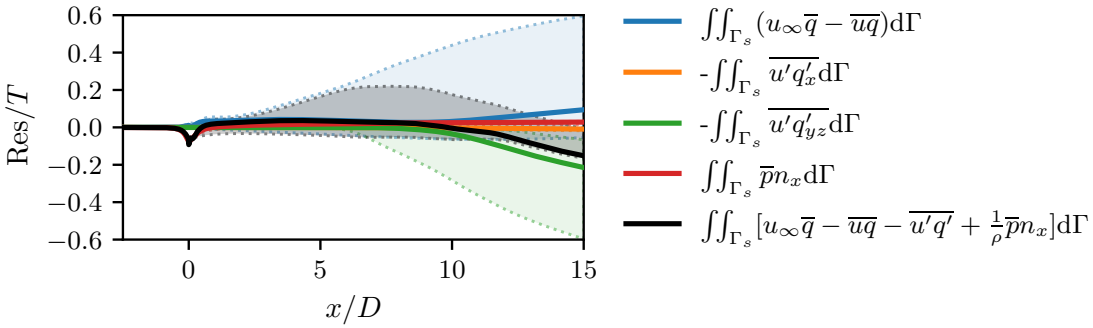

Figure 4. Streamwise evolution of the terms in the steady momentum-balance residual emerged from the assumption in Eq. (4), evaluated using the time-averaged LES data with the wake shape in an analytical actuator disc model and normalised by the rotor thrust. The shaded region, shown in the same colour as their corresponding curves and bounded by dotted lines, indicates the range of residuals obtained by scaling the wake width by a factor between 0.8 and 1.2.

5. Wake definition analysis

In this section, the wake definitions are assessed with various metrics. First, the physical consistency of the definition variants is evaluated using a steady momentum balance analysis. Then, the retained variants are assessed with the indices presented in Table 2 using the unsteady wake dataset. Lastly, the impact of wake definitions on the time-averaged wake statistics is presented.

5.1. Steady momentum balance analysis

The steady momentum balance relation in Eq. 3 is evaluated for different wake definitions using the time-averaged LES data. Figure 5 shows the change of F_w/T ratio for different variants of VelT, VelDefT, TT, and Gauss wake definitions. For the Gauss definition, only the Gauss (2D) results are shown, as the other Gauss variants of f_G yield nearly identical results. The tolerance $\eta_T = 0.2$ is also highlighted in the plots.

Many proposed variants are not suitable for this case as the resulting wake shapes cannot balance the turbine thrust within $\pm\eta_T$. The following variants, satisfying the $F_w/T = 1 \pm 0.2$ tolerance, are retained for unsteady analysis: VelT-0.95, VelT-0.98, VelT-1, VelDefT-0.01, VelDetT-0.05, TT-0.01, TT-0.1, Gauss-2σ and Gauss-3σ. Here, the value following the hyphen denotes the iso-contour threshold for the VelT, VelDefT, and TT definitions, and the wake half-width for the Gauss definitions. It should also be emphasised that all retained variants exhibit a monotonic decrease in F_w/T for $x/D > 7$, consistent with the residual analysis discussion in § 4.1.

5.2. Unsteady analysis

Figure 6 shows the streamwise variation of χ_c for different wake definitions. The majority of wake definitions yield $\chi_c > 0.99$. The exceptions are the TT-0.1, VelT-1, and MinP definitions, which typically yield much greater temporal variation in the lateral wake centre between consecutive snapshots. CoM-1, Gauss (2D) and Gauss (Biv.) definitions perform slightly better than the rest.

The streamwise distribution of χ_w is shown in Fig. 7. In the near wake, where the wake stays coherent, all the definitions lead to $\chi_w = 1$. As the wake begins to break down at

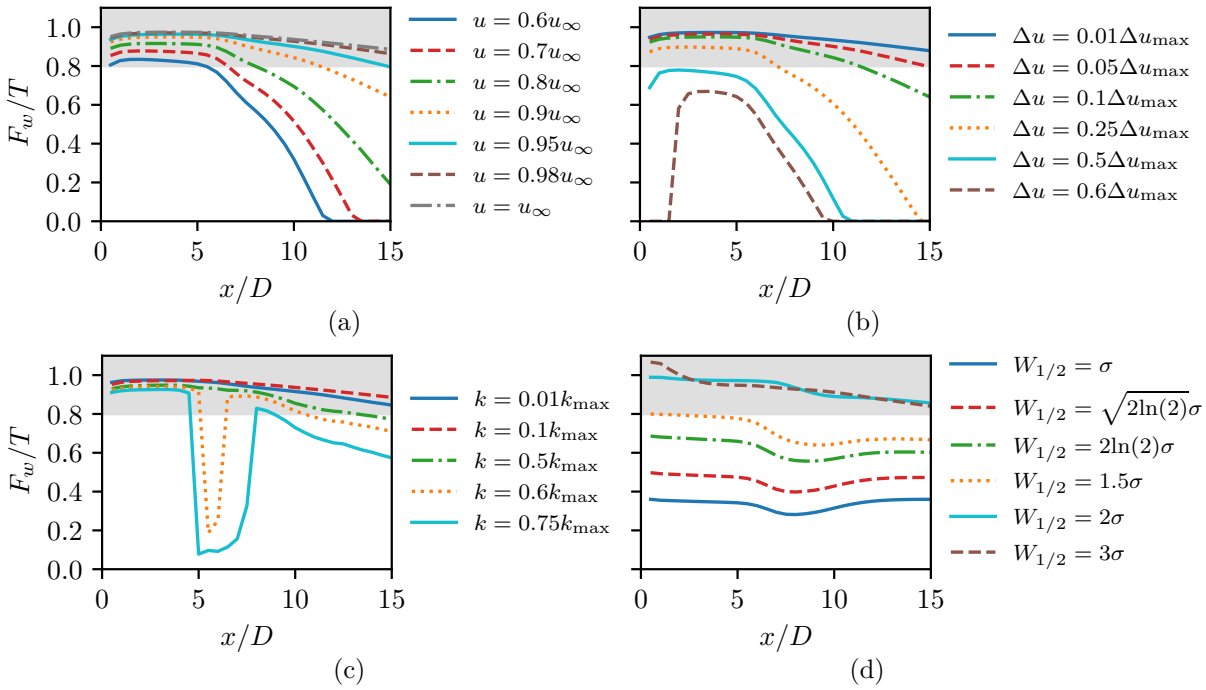

Figure 5. Streamwise variation of momentum balance ratio in the wake for different variants of (a)VelT, (b) VelDefT, (c) TT and (d) Gauss (2D) definitions. The grey shaded area represents the adopted tolerance for the momentum balance analysis.

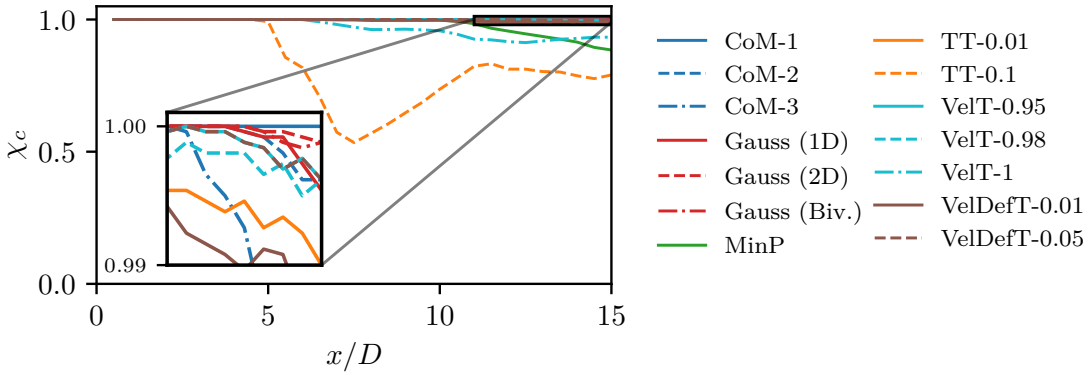

Figure 6. Streamwise variation of the wake centre index χ_c for different wake definitions, with an inset providing a magnified view of the region $11 \leq x/D \leq 15$ and $0.99 \leq \chi_c \leq 1$.

$x/D \approx 5$, the wake shapes identified by the TT-0.1 definition become unreliable. This behaviour is attributed to secondary turbulent structures shed from the shear layer in this region, which are known to contain highly localised peaks of turbulent kinetic energy [30]. Consequently, the TT definition with a relatively large definition metric may be biased toward identifying these localised structures as the whole wake rather than the entire wake region. In addition, the Gauss-3σ definitions exhibit poor performance in the far wake because they estimate unphysically large values of W_{eff}. Similar to the behaviour observed for χ_c, the f_G variants of Gauss definition yield nearly identical χ_w distributions. Across the examined domain, VelDefT-0.01 and VelT-1 definitions perform best, followed closely by VelT-0.98 and TT-0.01, primarily due to their superior performance on the momentum balance criterion.

These results indicate that velocity-threshold–based definitions with low deficit thresholds (e.g., VelDefT-0.01 and VelT-1) yield the most robust performance for instantaneous wake-shape identification. While the centre-of-mass and Gaussian-based methods yield reliable wake centre identification, the latter type may overestimate effective wake width in the far wake. Furthermore, definitions based on large turbulence thresholds should be used with caution in unsteady wake regions, where secondary turbulent structures undermine their validity.

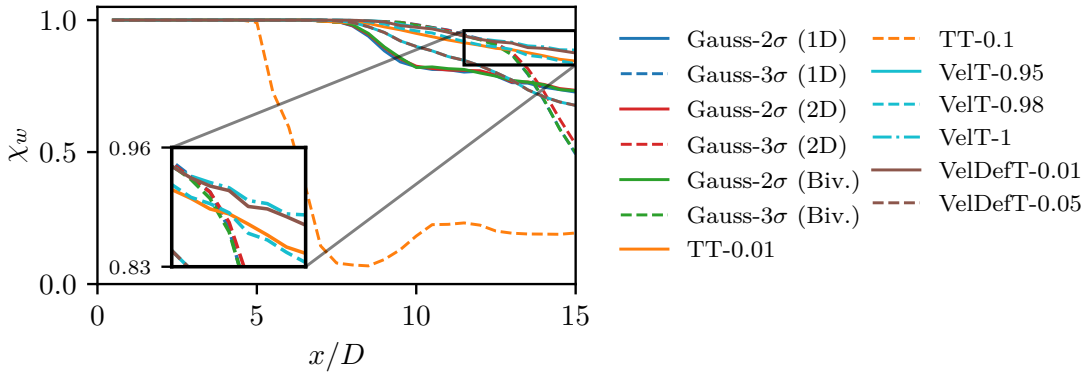

Figure 7. Streamwise variation of the wake shape index χ_w for different wake definitions, with an inset providing a magnified view of the region $11.5 \leq x/D \leq 15$ and $0.83 \leq \chi_w \leq 0.96$.

5.3. Time-averaged wake statistics

Time-averaged wake statistics, such as the wake growth rate and wake meandering amplitude, are typically used to calibrate engineering wake models. Since a wake definition determines these parameters, the specific choice of definition can strongly influence the model calibration.

Table 3 compares the wake growth rate, $\dot{W}_{\text{eff}}$, among the wake definitions. $\dot{W}_{\text{eff}}$ is determined by fitting a first-order polynomial to the time-averaged W_{eff} for each wake definition in the far wake, $x/D \geq 10$. All regressions resulted in a coefficient of determination (R^2) greater than 0.95, indicating strong linearity in the wake expansion rate. However, the magnitude of $\dot{W}_{\text{eff}}$ varies substantially among definitions. For example, the VelT-0.95 definition yields a growth rate less than one-fourth of the one predicted by the Gauss-3σ (Biv.) definition. Significant sensitivity is also observed within individual definition groups. For instance, there is a nearly 150% jump in $\dot{W}_{\text{eff}}$ from VelT-0.95 to VelT-1 definition.

Table 3. Wake growth rate $\dot{W}_{\text{eff}}$ obtained from linear fits to the time-averaged effective wake width at $x/D \geq 10$ for different wake definitions.

Definition	VelT			VelDefT		TT	
Variant	0.95	0.98	1	0.01	0.05	0.01	0.1
$\dot{W}_{\text{eff}}$	0.035	0.054	0.083	0.050	0.035	0.095	0.065

Definition	Gauss (1D)		Gauss (2D)		Gauss (Biv.)	
Variant	2	3	2	3	2	3
$\dot{W}_{\text{eff}}$	0.099	0.148	0.097	0.145	0.100	0.150

A similar sensitivity to wake definition is observed in the statistics of wake meandering. Consistent with previous studies [22], the standard deviation of the lateral wake centre displacement, which indicates the wake meandering amplitude [9], increases approximately linearly

with downstream distance in the far wake, as shown in Fig. 8 for most of the examined wake definitions. However, the magnitude of the meandering amplitude varies significantly, ranging from approximately $0.5D$ to $1.4D$ with different wake definitions at $x/D = 15$ downstream of the turbine.

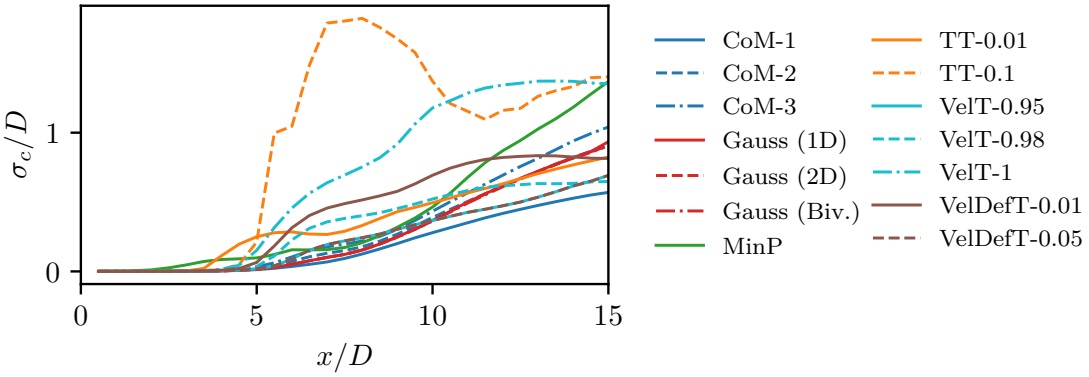

Figure 8. Streamwise variation of the standard deviation of the lateral wake centre shift for different wake definitions.

6. Conclusions

This study presents a quantitative assessment of several commonly used wind turbine wake definitions, focusing on their suitability for identifying instantaneous wakes. Using high-resolution LES data of an actuator disc, wake definitions are evaluated based on their ability to consistently determine the wake region and centre, and to generate wake shapes that satisfy momentum balance with respect to turbine thrust.

The steady momentum balance analysis using the time-averaged flow field shows that setting an inadequate metric for the wake definitions may lead to failure to satisfy the momentum balance within a reasonable tolerance of the applied thrust. As a result, the velocity threshold variants with $u/u_\infty \geq 0.95$, velocity deficit threshold variants with $\Delta u/\Delta u_{\max} \leq 0.05$, turbulent kinetic energy threshold variants with $k/k_{\max} \leq 0.1$, and Gaussian fit variants with the wake half-width defined by $W_{1/2} \geq 2\sigma$ are deemed to be physically consistent for the time-averaged wake as they generate wake shapes satisfying the momentum balance with the turbine thrust.

The retained wake definition variants are assessed using unsteady axial snapshots of the wake employing unified indices for the wake centre and shape. These indices are formed as the combination of multiple criteria for reliable and physically consistent wake identification. For the wake centre identification, all the considered definitions perform quite reliably, with centre-of-mass and Gaussian-based definitions exhibiting slightly better performance. In contrast, wake shape identification is more sensitive to the choice of definition. Velocity-threshold–based definitions with low deficit thresholds, such as the velocity threshold definition with $u/u_\infty = 1$ and the velocity deficit threshold definition with $\Delta u/\Delta u_{\max} = 0.01$, provide the most robust performance, as they maintain consistency with the momentum balance while limiting sensitivity to localised turbulent structures. Gaussian-based approaches remain appropriate for wake-shape identification, but may yield unphysically large effective wake widths. It should be noted that the recommendations and discussions in this study are derived from actuator-disc simulations under uniform inflow conditions. Their general validity for cases with turbulent inflow, realistic spanwise loading, or support structures may vary and requires further investigation.

Time-averaged wake statistics further revealed that the wake expansion and wake meandering statistics vary substantially with the chosen definition, suggesting that the choice of wake definition is not merely a methodological detail for wake identification, but a critical modelling decision that may influence conclusions drawn from wake instability analyses and engineering wake model calibration.

Acknowledgements

The authors acknowledge the support of CRV's UKRI Future Leaders Fellowship (MR/V02504X /1) and AAA's studentship from the Oxford Centre for Islamic Studies Scholarship. The authors would like to acknowledge the use of the University of Oxford Advanced Research Computing (ARC) facility (http://dx.doi.org/10.5281/zenodo.22558) and ARCHER2 UK National Supercomputing Service (https://www.archer2.ac.uk) through the EPSRC Access to HPC Call project e929 - Wake Aerodynamics of Offshore Wind Turbines (WAFT).

References

[1] Kang S, Yang X and Sotiropoulos F 2014 *J. Fluid Mech.* **744** 376–403
[2] Wang Y, Zhao G, Liu G, Zhou Y, Ge M, Ouyang Z, Ding Z and Hu R 2025 *J. Fluid Mech.* **1014** A3
[3] Adam A A, Vogel C and Smyth A 2025 *XI Int. Conf. Comput. Meth. Mar. Eng.* (Edinburgh, Scotland)
[4] Mao X and Sørensen J N 2018 *J. Fluid Mech.* **846** 190–209
[5] Gambuzza S and Ganapathisubramani B 2023 *J. Fluid Mech.* **963** A19
[6] Coquelet M, Gutknecht J, Van Wingerden J, Duponcheel M and Chatelain P 2024 *J. Phys. Conf. Ser.* **2767** 092084
[7] Xie S and Archer C 2015 *Wind Energy* **18** 1815–1838
[8] Schottler J, Bartl J, Mühle F, Sætran L, Peinke J and Hölling M 2018 *Wind Energy Sci.* **3** 257–273
[9] Yang X and Sotiropoulos F 2019 *Energies* **12** 4725
[10] Jézéquel E, Blondel F and Masson V 2022 *J. Phys. Conf. Ser.* **2265** 022067
[11] Fan Z, Li S, Gao Z, Zhang L, Zheng X, Zhu W, Shen W, Sjöholm M, Mikkelsen T K, Wang T and Li Y 2023 *Energy Convers. Manage.* **277** 116664
[12] Coudou N, Moens M, Marichal Y, Van Beeck J, Bricteux L and Chatelain P 2018 *J. Phys. Conf. Ser.* **1037** 072024
[13] Quon E W, Doubrawa P and Debnath M 2020 *J. Phys. Conf. Ser.* **1452** 012070
[14] Krutova M, Bakhoday-Paskyabi M, Reuder J and Nielsen F G 2022 *Wind Energy Sci.* **7** 849–873
[15] Fei Z, Nishino T and Vogel C 2025 *J. Phys. Conf. Ser.* **3016** 012033
[16] Zormpa M, Adam A A, Willden R H J and Vogel C R 2025 *J. Phys. Conf. Ser.* **3016** 012031
[17] Hölling M *et al.* 2025 *J. Phys. Conf. Ser.* **3016** 012013
[18] Poletto R, Craft T and Revell A 2013 *Flow Turbul. Combust.* **91** 519–539
[19] Vinnes M K, Gambuzza S, Ganapathisubramani B and Hearst R J 2022 *J. Renewable Sustainable Energy* **14** 023304
[20] Howland M F, Bossuyt J, Martínez-Tossas L A, Meyers J and Meneveau C 2016 *J. Renewable Sustainable Energy* **8** 043301
[21] Brucker K A and Sarkar S 2010 *J. Fluid Mech.* **652** 373–404
[22] Hodgson E L, Madsen M H A and Andersen S J 2023 *Phys. Fluids* **35**(9) 95125
[23] Howard K B, Singh A, Sotiropoulos F and Guala M 2015 *Phys. Fluids* **27** 075103
[24] Foti D, Yang X and Sotiropoulos F 2018 *J. Fluid Mech.* **842** 5–25
[25] Barthelmie R and Pryor S 2013 *Appl. Energy* **104** 834–844
[26] Trujillo J, Bingöl F, Larsen G C, Mann J and Kühn M 2011 *Wind Energy* **14** 61–75
[27] Bempedelis N and Steiros K 2022 *Phys. Rev. Fluids* **7** 034605
[28] Bastankhah M, Hydon P E, Shapiro C, Gayme D F and Meneveau C 2025 *arXiv preprint arXiv:2510.08213*
[29] Lignarolo L E M, Ragni D, Scarano F, Simão Ferreira C J and van Bussel G J W 2015 *J. Fluid Mech.* **781** 467–493
[30] García-Villalba M, Fröhlich J and Rodi W 2006 *Phys. Fluids* **18** 055103